Three dimensional tracking of multiple objects using digital holographic microscopy

Anton Abrahamsson

August 23, 2016

Abstract

Measuring micro-fluidic flows and its characteristics is important when designing and developing lab-on-the chip technologies. Commonly, micro-spherical particles are introduced in the flow and the velocity of the particles provide information of the flow profile. By measuring the position of a particle the local flow velocity can thus be determined. To measure the position of a particle in 3D, digital holography is a powerful technique that samples holograms and use digital reconstruction to find spatial information of the particle. This work presents a three dimensional tracking approach based on digital holographic microscopy, that is cheap and simple to implement. A cross correlation algorithm is used to track the object in the x,y-plane whereas the z-position is found using Rayleigh–Sommerfeld back-reconstruction theory. The algorithm was tested on both synthetic holograms, generated by ray-tracing software, and on spherical polystyrene micro-spheres in a micro-fluidic chamber using both stationary and flowing water. The results show that the beads in the micro-fluidic chamber could be tracked with high accuracy, with a standard error of approximate 0.003 μm and 0.05 μm in the x,y-plane and z-plane (reconstructed distance), respectively. For the latter, this worked fine as long as the diffraction patterns where relatively undisturbed. Noise and resolution of the image limits the accuracy of the tracking of the center position as well as the z-position by reconstruction.

Client: The Biophysics and Biophotonics group, Umeå University
Supervisor: Hanqing Zhang
Examiner: Magnus Andersson

Tredimensionell spårning av flera objekt med hjälp av digital holografisk mikroskopi

Sammanfattning

Att mäta mikroflöden är viktigt nära man designar och utvecklar teknologier för lab-on-the chip ändamål. Ofta så använder man sig av mikrosfärer i flödet och hastigheten på partiklarna ger information om flödesprofilen. Genom att mäta positionen på partiklarna, kan det lokala flödet bestämmas. Den tredimensionella positionen av partiklar kan mätas genom digitalt holografi. Detta examensarbete presenterar en billig och enkel metod, samt en algoritm för att spåra den tredimensionella positionen av partiklar genom digitalt holografiteknik. En kors-korrelations algoritm används för att följa objekten i x,y planet medan z positionen erhålls med Rayleigh–Sommerfeld rekonstruktions teori. Algoritmen testades på både syntetiska hologram, skapade i ray-tracing mjukvara och på mikrosfärer i en mikroflödes kammare, där både stillastående och flödande vatten användes. Resultaten visade att sfärerna kunde följas med en hög precision, standardavvikelsen var ca 0.003 μm i x,y planet och 0.05 μm i z planet (den rekonstruerade distansen). För att få hög noggranhet hos den rekonstruerade distansen så behövde diffraktionsmönsterna vara fri från störningar, dvs brus och upplösningen på bilden begränsar precisionen på positionen i både x, y och z.

Contents

1 Introduction

1.1 Background

Microfluidics is a multidisciplinary field, where a small quantity of fluid is flowing through a lab-on-the-chip (LOC) device, which in principle, integrates several analyzing functions on one small chip. Typical applications are; enzyme synthesizing, chemical detection, and a common tool in microbiology is to measure adhesion forces of individual cells. Due to the small volumes in a flow chamber, μl, and the small size of the objects flowing in a LOC, it is difficult to quantitatively measure the forces directly. Thus, there is a need of methods that are able to find the three dimensional position, velocity and shape of an object in order to estimate the net force on an object in a LOC device.

Digital holographic microscopy (DHM), is an imaging technique that has many practical application since it has the ability to capture and reconstruct holograms digitally, which has replaced the photo-chemical process that was used in conventional holography[1]. The reconstruction can be made using any diffraction theory of which the most commonly used is the Rayleigh-Sommerfeld, since the fast calculation time of modern computers has removed the need to use the Fresnel and the Fraunhofer approximation. The Rayleigh-Sommerfeld theory only require some boundary condition to be valid[2][3]. The integral in the Rayleigh-Sommerfeld theory can be numerically evaluated using either direct integration or the angular spectrum method[2].

The main advantage of DHM over conventional microscopy is that the hologram contain information about both the amplitude and the phase of an object, resulting in that focusing is made during the numerical reconstruction, making it easy to refocus. However, the criteria of the focus has been determined externally[4]. In this work, the focus was chosen to the distance with the highest intensity at the center of the diffraction pattern. This criteria give a computationally inexpensive measure of the distance to the focus of the object. The ability to estimate focus after the measurement, make DHM suitable to track moving microscopic objects. Digital holography also have the ability to provide a detailed 3D structure of an object, making it useful to measure small movements in bigger objects[5][6]. In addition, DHM is a powerful tool in microbiology, where this noninvasive technique has been used to measure cell structure with high resolution, cell shape as well as parameters like refractive index and thickness of cells[7][8][9]. DHM has also been used to study migration and morphology of cell clusters[10][11][12].

1.2 Aim of thesis

The first aim of this work is to develop, refine and verify an algorithm that can track the three dimensional position of multiple spherical micro-particles in a microfluidic chamber. The algorithm should be written in Matlab and consist of one part that can accurately find the two dimensional lateral position and another part that can reconstruct the axial position from a hologram.

The second aim of this work is to develop and implement an experimental setup that is able to measure holograms from micro-spheres in a micro-fluidic flow that should be: cheap, simple and build around an existing microscope in the Biophysics and Biophotonics group. Finally, the algorithm should be validated using both synthetic and experimental holograms.

2 Theory

2.1 Holographic reconstruction

In conventional brightfield microscopy the object is illuminated using a white light source and the object is positioned in the focus of the objective. In contrast, in DHM the object is illuminated by a quasi monochromatic light source and scattered light from the object interfere with undisturbed light from the source. The position of the focus of the object is then obtained by numerically back-reconstructing using information from the diffraction pattern to get the image.

One commonly used holographic setup is Gabor holography, were a single beam of monochromatic light is used to illuminate the object. The object will scatter the light and the scattered and non scattered light will interfere and create a diffraction pattern. Fig 1 shows the principle of imaging holograms. Since the reconstruction refers to the focus of the object the reconstructed distance will underestimate the real distance to the image plane.

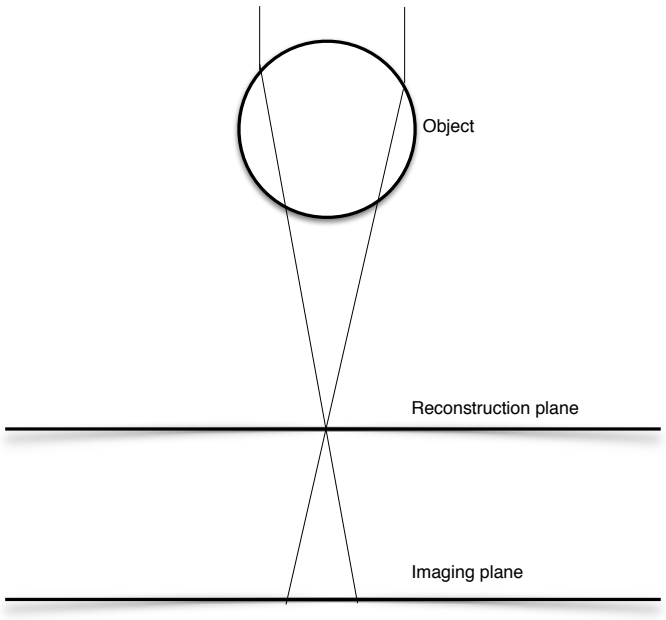

Figure 1: Principle of holography. The light is diffracted at the object and the light is captured at the imaging plane. The object is then reconstructed at the reconstruction plane.

No separate reference wave is used in Gabor holography implying a simple setup, however, the object must be small and weakly diffractive for Gabor holography to work [13]. Since there is no angle between the scattered and non-scattered light, Gabor holography is refered to an in-line configuration [1] and the intensity I on the detector is given by

$$I = |U_O + U_R|^2 = |U_O|^2 + |U_R|^2 + U_O U_R^* + U_O^* U_R, \tag{1}$$

where U_R is the non-scattered amplitude and U_O is the scattered amplitude, * denotes a complex conjugate. On the right hand side of the equation, the first two terms are the zero order terms, the two remaining terms are the real and conjugate image. Typically the scattered amplitude is much smaller compared to the non scattered amplitude.

For a monochromatic wave the field u can be written as

$$u(x, y, z, t) = RE(U(x, y, z)e^{i\omega t}), \tag{2}$$

where ω is the angular frequency of the wave, t is the time, x, y and z is the spatial position, i is the imaginary unit and U is the complex amplitude of the wave, that obeys the Helmholtz equation

$$(\nabla^2 + k)U(x, y, z) = 0, \tag{3}$$

where k is the wave number and ∇^2 is the Laplacian.

Rayleigh-Sommerfeld diffraction theory is based on the geometry in Fig. 2, where light is traveling in the positive z-direction through the planar surface S_0, located in the $z = 0$ plane right behind an aperture. S_ϵ is a sphere surrounding the point of interest, P and S_1 is an arbitrary surface in the positive z region.

$$\int\int_{S_0} (U\nabla G - G\nabla U)\cdot\hat{n}ds_0 + \int\int_{S_\epsilon} (U\nabla G - G\nabla U)\cdot\hat{n}ds_\epsilon + \int\int_{S_1} (U\nabla G - G\nabla U)\cdot\hat{n}ds_1, \tag{4}$$

where G is a Green function, that obey the Helmholtz equation and $\hat{n}$ is the normal vector pointing outward on the boundary. By applying Green's theorem and the fact that both U and G obey the Helmholtz equation, the integral (4) becomes 0. By expanding S_1 to infinity and using the Sommerfeld radiation condition that part of the integral will give zero contribution. By shrinking down S_ϵ to zero, the integral becomes

$$\int\int_{S_\epsilon} U\nabla G - G\nabla U \cdot \hat{n}ds = 4\pi U(P), \tag{5}$$

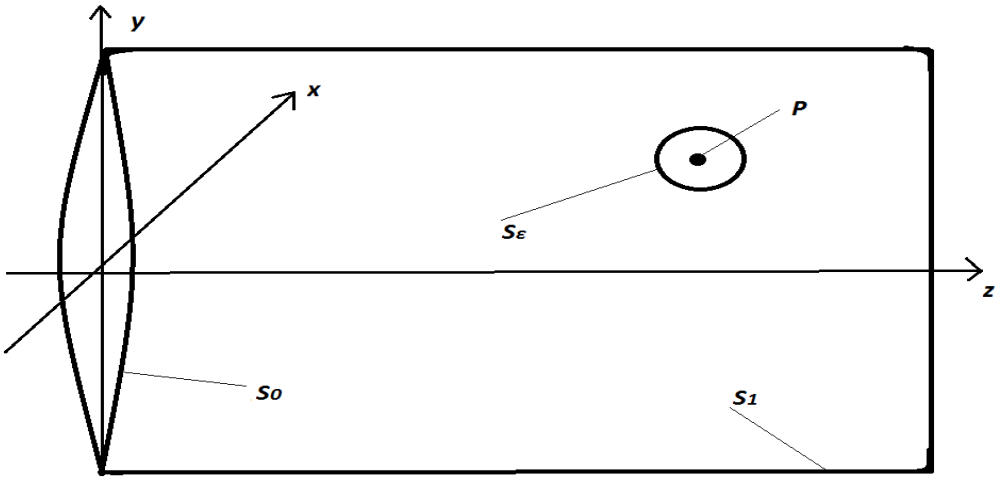

Figure 2: Geometry used to establish the diffraction theory

resulting in

$$U(p) = \int\int_{S_0} U\nabla G - G\nabla U \cdot \hat{n} ds. \tag{6}$$

The Rayleigh-Sommerfeld theory apply the following boundary condition,

$$U(x, y, 0) = U_0(x, y, 0), \tag{7}$$

for transmissive parts, where U_0 is the incident wave and

$$U(x, y, 0) = 0, \tag{8}$$

for blocking parts. These approximations gives the Green function

$$G = \frac{exp(jk(r_2 - r_0))}{r_2 - r_0} r - \frac{exp(jk(r_1 - r_0))}{r_1 - r_0}, \tag{9}$$

where r_0 is the vector to a point on the z=0 plane, r_1 is the vector to P and r_2 is the vector to the mirror image of P.

By setting in G from equation (9) in equation (6), the diffraction integral becomes

$$U(P) = \frac{-ikz'}{2\pi} \int_{Area} U_0(x, y, 0) \frac{exp(ikr)}{r^2} (1 - \frac{1}{ikr}) dxdy, \tag{10}$$

where $r = ((x-x')^2+(y-y')^2+z'^2)^{0.5}$, z' is the axial distance between the hologram plane and reconstructing plane, x, y, x' and y' are the coordinates of the hologram and reconstruction plane. If one also assume that $r \gg \lambda$, where lambda is the wavelength of the light, one get the Rayleigh-Sommerfeld approximation model

$$U(P) = \frac{-ikz'}{2\pi} \int_{Area} U_0(x,y,0) \frac{exp(ikr)}{r^2} dxdy. \tag{11}$$

In the angular spectrum method the wave is represented as a sum of planar waves. With this equation (11) becomes

$$U(P) = \frac{-ikz'A_0}{2\pi} \int_{Area} \frac{exp(i(k_x(x-x') + k_y(y-y') \pm k_z z))}{r^2} dxdy, \tag{12}$$

where A_0 is the amplitude of U_0 and k_x, k_y and k_z are the components of k. This is a convolution integral, so the propagation can be handled in the frequency domain. The diffraction pattern U is expressed as [2]

$$U(x',y',z') = F^{-1}[F(U(x,y,0) \cdot h(k_x,k_y,z'))], \tag{13}$$

where F denote Fourier transform, F^{-1} denote inverse Fourier transform and h is the transfer function of free propagation, that is given by,

$$h(x',y',z') = exp[iz'\sqrt{k^2 - x'^2 - y'^2}]. \tag{14}$$

2.2 Cross correlation

To reconstruct an object the lateral position of its diffraction pattern in the hologram has to be found. One way to estimate the change in lateral position of an object between two frames is by using cross-correlation that is a measure of how similar two matrices are when one of the matrices is shifted. The 2D discrete cross correlation is defined as

$$(F \star G)(k,l) = \sum_{m=-\infty}^{\infty} \sum_{n=-\infty}^{\infty} F(m,n)G^*(m+k,n+l). \tag{15}$$

If the matrices are real and both F and G has the finite size of $M \cdot N$, the cross correlation is calculated by

$$(F \star G)(k,l) = \sum_{m=0}^{M-0} \sum_{n=0}^{N-1} F(m,n)G(m+k,n+l), \tag{16}$$

where $-(M-1) \leq k \leq (M-1)$ and $-(N-1) \leq l \leq (N-1)$.

If F and G differ from each other in that one of them is shifted, the location of the maximum in the cross-correlation will determine the shift between F and G[14], hence the odd indexing of the matrix, a positive index correspond to a upward or leftward displacement.

2.3 Laminar flow

The flow velocity experienced by an object in a channel depend on where in the channel the object is located. When the flow is laminar the fluid will flow in parallel layers and there will not be any mixing between these layers, which is valid when the flow channel is small and the flow velocity is low and the viscosity of the fluid is high. The velocity profile of a laminar flow in a long straight tube will have a parabolic shape and can be described by,

$$V(r) = V_m(1 - \frac{r^2}{R^2}), \tag{17}$$

where V is the velocity, V_m is the velocity at the center of the tube, R is the radius of the tube.

3 Algorithms used

3.1 x and y position tracking

The tracking algorithm is applied for each frame. Details of the tracking are presented as a pseudo code below.

Create a binary mask where values over a set threshold will be set to 1.
Fill any holes in the binary mask.
Remove smaller areas in the binary mask.
Take out the center of all areas, by using their centroids.
if The frame is the first one **then**
    Show both the image and the final binary image to the user, with the centriods marked.
    Let the user remove any objects from the tracking.
    Create trackers containing information of the position.
    Use the centroids to get their x and y position and cut out a template of the binary object.
Take out the distance between all objects
for All trackers **do**
    Cut out all objects from the binary mask on the position they were on the last frame
    if There is no object there **then**
        Put the x and y position to NaN and stop the tracking after this frame.
    else
        Find the relative position shift in x and y, by finding the maximum value in the cross correlation (16) between the template and the cut out object.
        Update the x and y position of the object.
    if The object is neither too close the edge nor too close to another object **then**
        Take out the object and reconstruct its z position.
    if The frame is the first one **then**
        set the speed to NaN.
    else if The z position on this and the previews frame is known **then**
        Calculate the speed, given in spherical coordinates.
    else
        Calculate the speed, given in polar coordinates.
    if The object is close to a edge **then**
        Stop tracking the object after this frame.

28: Save the tracks. See appendix for details.
The x, y-tracking algorithm have the following inputs:

- A video file of the objects.
- A background image.
- The wavelength of the light source.
- The frame rate of the camera.
- A conversion factor from pixels to meters.
- A threshold for the binary mask
- A thresholds for how close a object can be to the edge and other objects.

3.2 Reconstruction algorithm

1: Refine the center of the object.
2: Put the object into a median value frame.
3: Calculate the size of the frame.
4: Fourier transform the frame.
5: **if** The reconstructed distance of the last frame is not known **then**
6: Calculate the transfers function of free propagation accordingly to equation (14) and calculate the propagation of the diffraction pattern accordingly to equation (13) for z from 0 to 100μm with a resolution of 7μm.
7: Calculate the z position where the reconstructed intensity has the highest value along the z axis at the center of the diffraction pattern.
8: fine tuning using the same calculation as step 7 and 8 with a resolution of 700 nm.
9: Calculate the transfers function of free propagation accordingly to equation (14) and calculate the propagation of the diffraction pattern accordingly to equation (13) for z around the maximum that was found or from the previous frame with a resolution of 70 nm.
10: Calculate the z position where the intensity were highest at the center of the diffraction pattern.

The algorithm is prevented to reconstruct away from the object. The frame is used to prevent oscillations in the intensity at the center of the diffraction pattern [2]. Currently the reconstruction algorithm can not handle jumps in the z direction larger than 450 nm from one frame to the next, it is simple to remove this limit but a smaller limit will result in faster reconstruction.

4 Experimental procedure

4.1 Setup

The DHM setup was build around an Olympus IX70 inverted microscope, normally used for tissue culture application and optical tweezers experiments [15][16][17]. The original setup of the microscope was modified so that instead of using the inbuilt brightfield lamp, a quasi monochromatic light emitting diode (LED) with a wavelength of 470 nm was applied. The LED (M470F1, Thorlabs), was connected via a SMA fiber connector using the butt-coupling technique. A optical fiber (M28L02, Thorlabs) was used to guide the light and to get a collimated beam a output collimator (PAF-SMA-7-A, Thorlabs) was used. The Collimator was positioned so that the sample was iluminated from above using a custom built holder. To control the LED, a LED driver (LEDD1B, Thorlabs) that can provide a maximum current amplitude of 0.7 A, was used. The holder was positioned on a piezo controlled stage (P-561.3CD, Physik Instrumente), which had sub-nm position resolution and was connected to a controller unit (E-725, Physik Instrumente) and steered via the software (PIMicroMove) to set the position. The piezo controlled microscope stage was placed on a step-motor stage that could be manually moved using a controller unit (MultiControl 2000, Märzhäuser Wetzlar) connected with a joystick (JoystickHD, Märzhäuser Wetzlar). Fig. 3 shows the schematics of the setup [8].

4.2 Sample preparation

The sample objects were polystyrene mono size microspheres with a diameter of 2 μm (A37299, Thermo Fisher Scientific). Microspheres were mixed in ultrapure Mili-Q water with a resistivity of 18.2 MΩcm to get a preferable concentration. The concentration was chosen to have a low amount of beads in the field of view to avoid overlap in their diffraction pattern. The concentration in turn depended on the measurement that had been done, thus I used an trial-and-error approach to find the right concentration.

To measure the spheres in stationary water, a sample chamber were prepared using two cover slips (no. 1, Knittel Glass). A $60 \cdot 24$ mm cover slip where used as frame and two pieces of double sticky tape (Scotch) where placed on the cover slip to create a channel that was 5 mm wide. On top of the tape a $20 \cdot 20$ mm cover slip was placed. The sample, consisting of diluted microspheres in Mili-Q water, was injected into the chamber using a 10 μl pipett. The chamber was filled with sample fluid due to capillary forces. After loading samples into the chamber, the chamber was sealed by adding vacuum grease (Dow Corning) on both openings to prevent evaporation

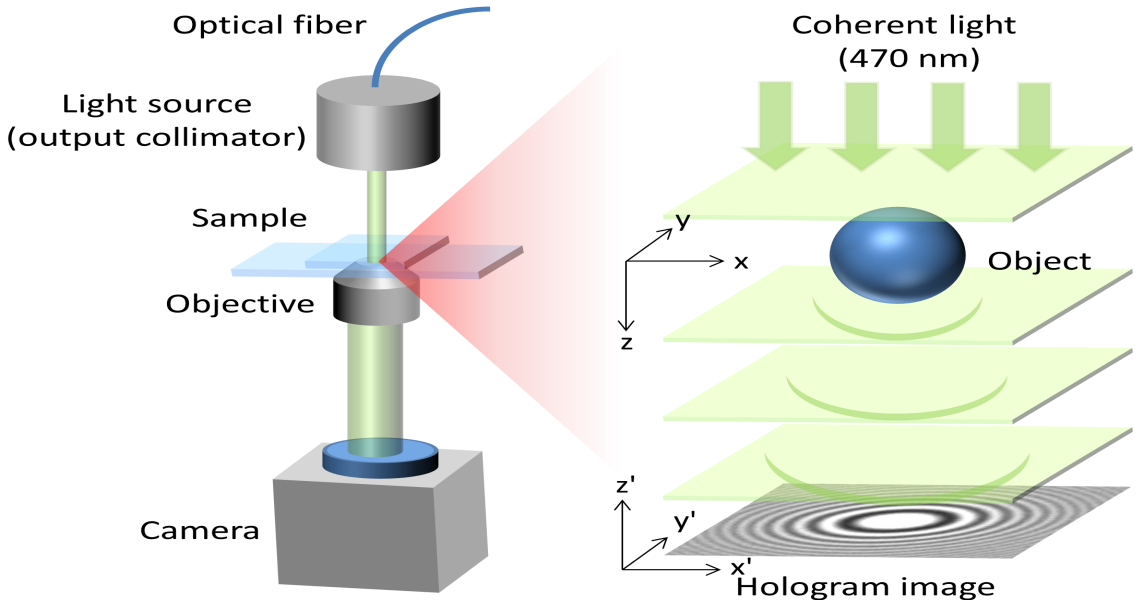

Figure 3: Schematic overview of the setup. Figure taken from reference [8].

that could result in unwanted movements of the microspheres. This type of chamber had been used in particle tracking and bacterial force studies and has been shown to be reliable[18][19][20][21].

To create a desirable flow chamber a commercial micro-fluidic chamber commonly implemented as a bio-chip (Vena8, Celix), which is 28 mm long, 400 μm wide and 100 μm high, was applied.

4.3 Measurement procedure

In general, a measurement was performed as follows. The sample was illuminated from the top and imaged with a water immersion object (UPlanSApo 60X, Olympus). By turning the object turret, so that the objective got slightly misaligned, the illumination in the region of interest got more even, as a bright spot in the background disappeared from the hologram.

A measurement in stationary conditions was performed by placing the sample chamber onto the microscope stage and illuminating the sample using the LED. A hologram was captured using a 12-bit CMOS camera (C11440-10C, Hamamatsu Photonics) positioned close to the eyepiece. The camera was controlled with the

software ICImageLive and the exposure time of the camera was set to 1 ms, allowing sufficient amount of light reaching the detector.

To measure the position and velocity of spheres in flowing water, the micro-fluidic chamber was put on the microscope stage and coupled to a microfluidic pump (Mirus Evo, Celix). The pump withdraw the solution of microspheres and water from a glass container and pumped it through the micro-fluidic chamber. The excess of the water was allow to flow freely to a glass container filed with tissue paper. The pump flow was controlled with the software VenaFluxAssay containing all commands needed to control the pump.

To acquire holograms with less distortion in the image due to fast moving particles, we switched the Hamamatsu camera to a high-speed camera (EoSens cube 7, MotionBLITZ) to able to run up to 1 640 frames per second at 1280 x 720 resolution. This camera was controlled by the software MotionBLITZDirector2 and the frame rate in a typical experiment was set to 200 Hz.

5 Results

5.1 Validation of the algorithm

The algorithm describe above was implemented in MATLAB, and to first validate the precision of the algorithm, synthetic holograms were generated in Zemax, which is a ray-tracing program. In the simulation, 10 spherical objects, with refractive index of 1.50 and radius of 3.50 μm were placed in water at distances 40, 50, 60, 70, 80, 90, 100, 110, 120 and 130 μm, from a virtual detector. A virtual detector in Zemax counts the amount of rays passing through a surface without affecting the propagating rays. Rays were generated from a coherent light source of 470 nm wavelength and 4 billion rays where traced in a simulation. The rays illuminated the objects coherently and the diffracted rays generated a hologram as is shown in Fig. 4.

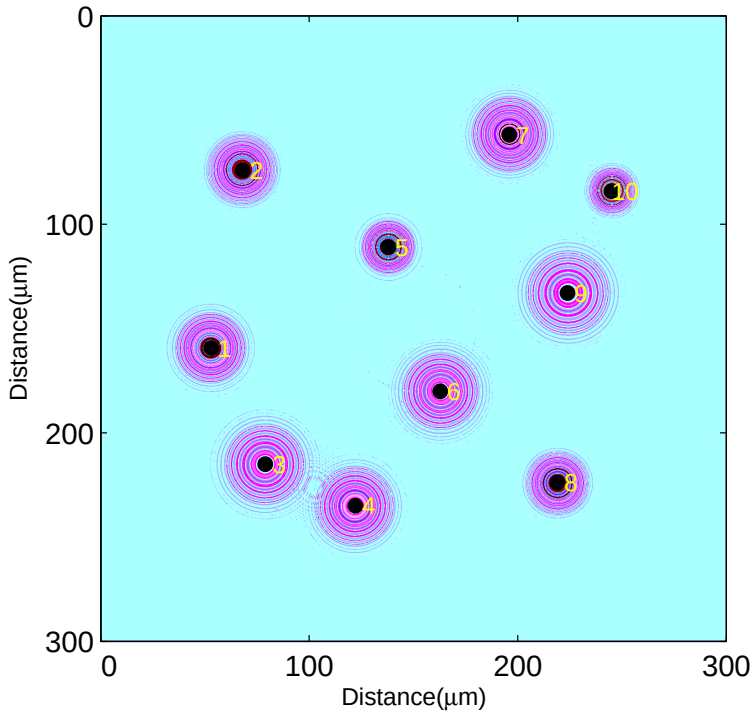

Figure 4: A synthetically generated hologram, using Zemax simulation software, of micro-spheres positioned at different heights and illuminated using a coherent light source. The detected center of each micro-sphere is marked with a number.

First, the tracking algorithm was used to test if it could find the center of the diffraction pattern. In Fig. 4 the centers of each particle is marked by a black dot and the diffraction pattern is clearly seen as the ring-like pattern surrounding the center. A small overlap are seen between the diffraction patterns of particle three and four, however the algorithm still found the center of all diffraction pattern.

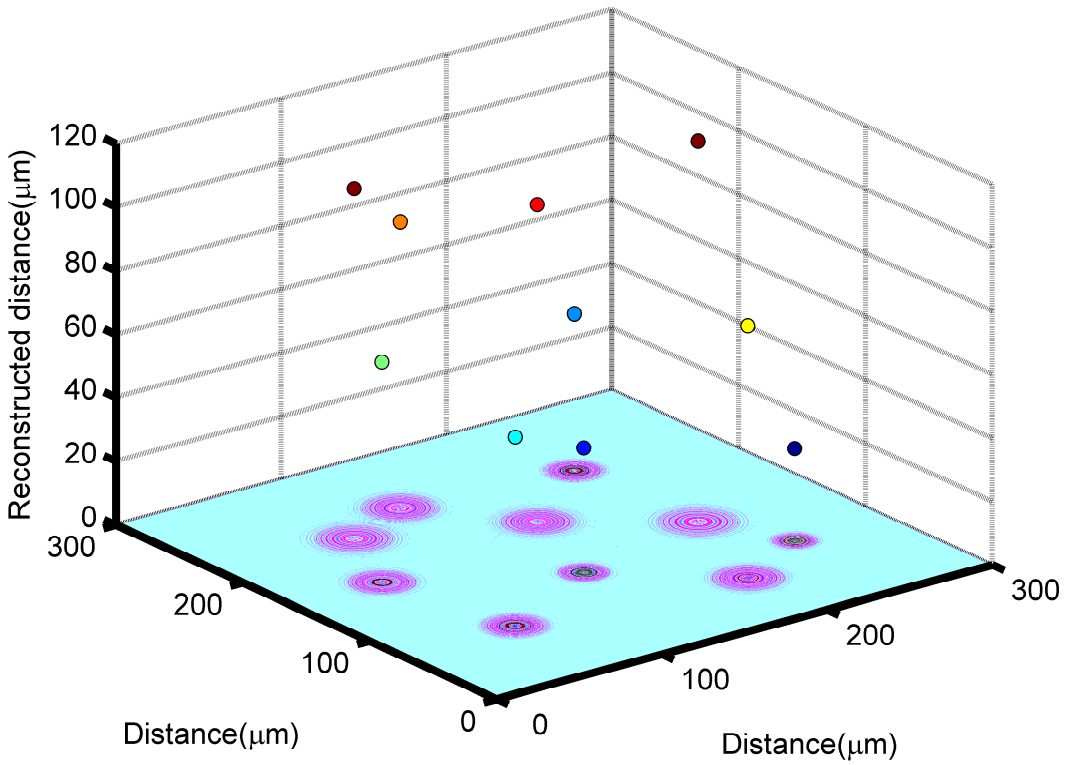

Figure 5: The reconstructed positions marked over the synthetic hologram.

Based on the found centers, the reconstruction algorithm was tested within an area around each center containing $201 \cdot 201$ pixels, corresponding to $8.84 \cdot 8.84$ μm. Such strategy allowed all the diffraction pattern to be covered entirely and the overlap was kept at minimum. Fig. 5 shows the generated hologram and the reconstructed position of the spheres. The reconstructed position are color coded after reconstructed distance.

In both Fig. 4 and Fig. 5, the distances on the x and y axis are only relative distance. We can therefore relate the relative distance from reconstruction to the ground truth distance from the Zemax simulation using a model. A linear model was chosen and the fitting showed a R^2 of 0.9999, and the p-value for the slope coefficient was smaller than 0.001, meaning that the reconstruction algorithm can predict the position of the particle accurately. Figure 6 shows the linear fit to the data. One can clearly see, as expected, that the reconstructed distance is smaller than the real distance. The two spheres that had overlapping diffraction pattern were placed 100 and 120 μm away from the detector and no abnormality can be seen on these data points.

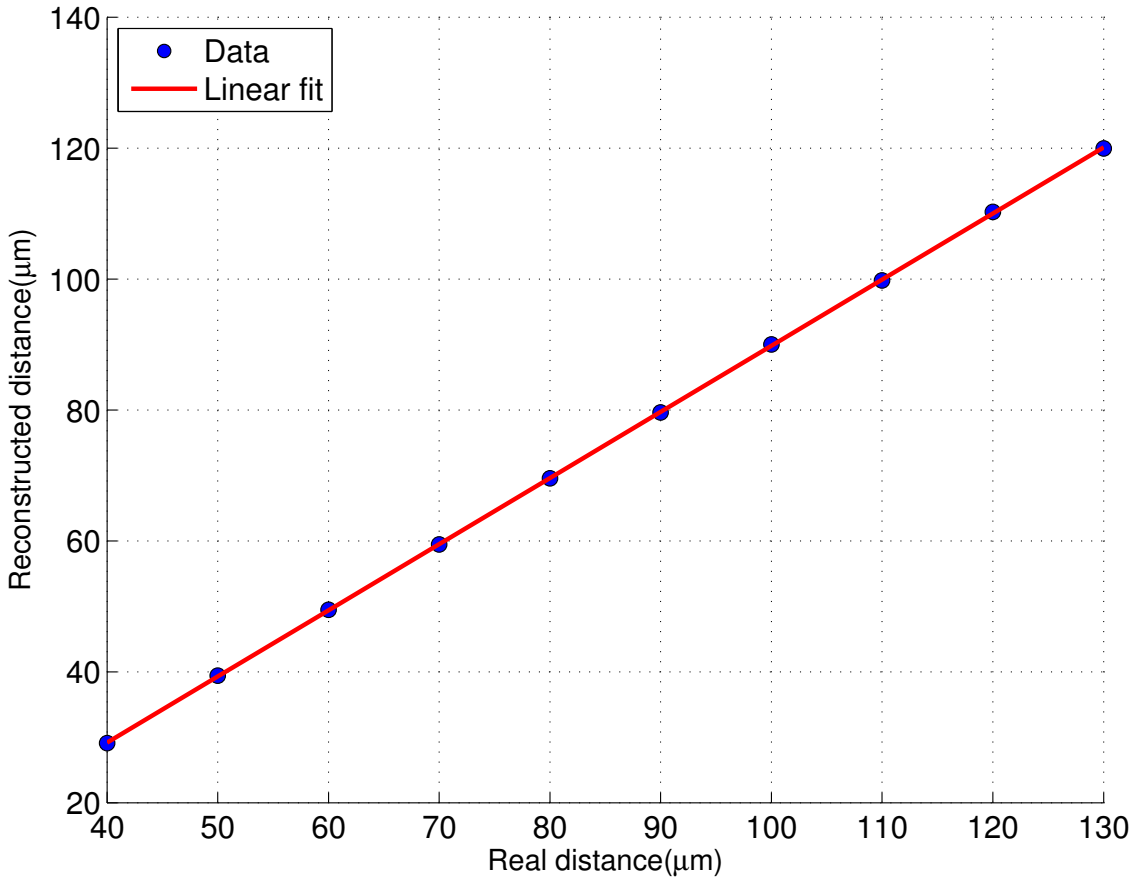

Figure 6: A linear fit between the real distance and reconstructed distance using data from the synthetic hologram.

6 Stationary test

Physical experiments were conducted to test that the algorithm could track an object over time. We used polystyrene micro-spheres sufficiently small to undergo Brownian motion. A sequence with one hundred images where taken, with a frame rate of 45 image per second. The pixel to meter conversion factor was found by placing a micrometer ruler in the microscope and counting the number of pixels between a given distance. The conversion factor of the setup was found to be 0.121 ± 0.008 μm. To get a evenly illuminated background, all frames were subtracted with a background image. The first subtracted frame in the sequence can be seen in Fig. 7(a), where the detected centers are marked by a blue dot. One can see that not all patterns (diffraction rings) were detected, as some pattern do not have any clear rings. The algorithm also fail to separate the two diffraction patterns that are close to each other and instead give only one center, see number 9 in the middle of the image, this object were excluded in the tracking. These two pattern are too close to each other to get any meaningful distance from the reconstruction.

In Fig. 7(b) frame 25 in the image sequence is shown, Fig. 7(c) shows frame 50 and Fig. 7(d) shows frame 75, one can see that some objects are detected in frame 25, 50 and 75 that where not detected during the first frame, object 11 in the first frame could be seen in the first 24 frames. Only diffraction pattern found during the first frame was analyzed.

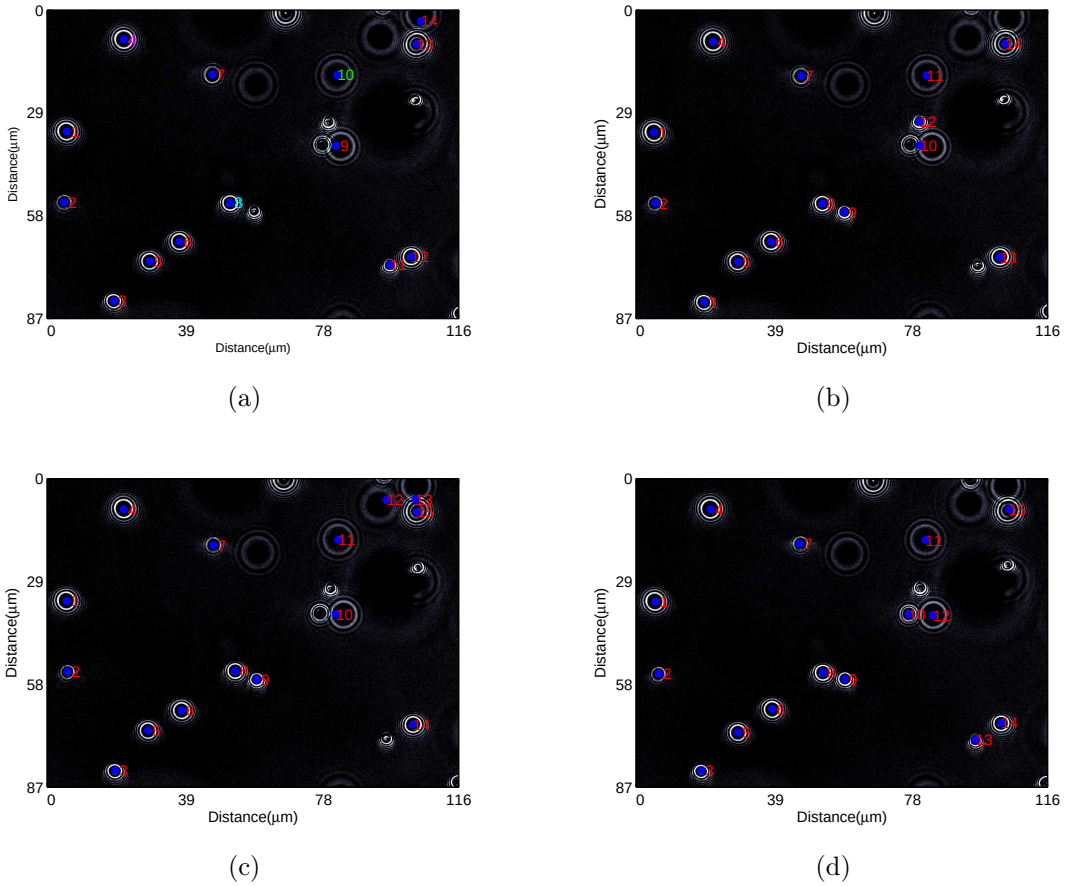

(a) (b)

(c) (d)

Figure 7: Frames from the image sequence from stationary test. (a) First frame. (b) Frame 25. (c) Frame 50. (d) Frame 75.

Fig. 8 shows the detected objects from Fig. 7(a) and as one can see object 10 is not detected as a solid object and object 14 is only partially in the frame. In the reconstruction an area of $121 \cdot 121$ pixels around the center was used. The position of the area and contents in the image were checked to avoid errors from the edges of the image and from diffraction patterns from other objects.

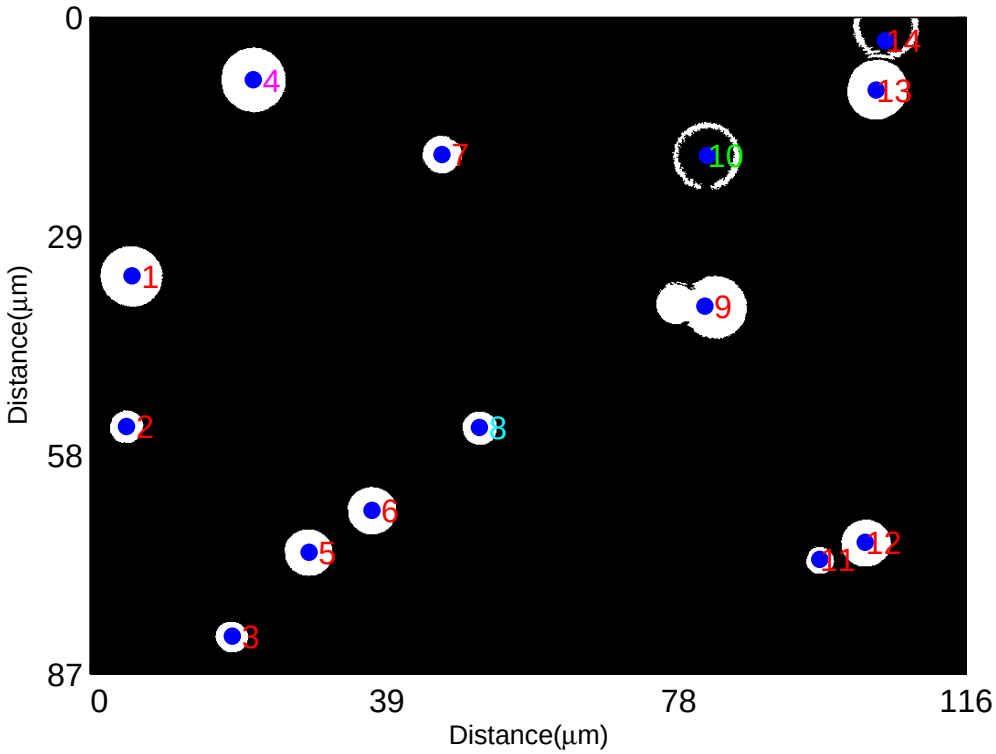

Figure 8: The objects that were detected in the first frame in the image sequence with their center marked.

The reconstructed distance over 2.2 seconds for object 4, 8 and 10, can be seen in Fig. 9. The data shows that object 10 is further away, that is higher up from the cover slip, compared to object 4 and 8. The average reconstructed position is; for object 4; 7.76 ± 0.08 μm, for object 8; 4.9 ± 0.1 μm and for object 10; 25.3 ± 0.2 μm.

In Fig. 7(a) one can see an undetected object in proximity of object 8. This can give rise to problems since the diffraction patterns can overlap making it hard to

properly reconstruct the height. Examples of failed reconstructions are the data for object 11, 12, and 13, as well as object 1, 2, 3 and 14, which are too close too the edge of the image.

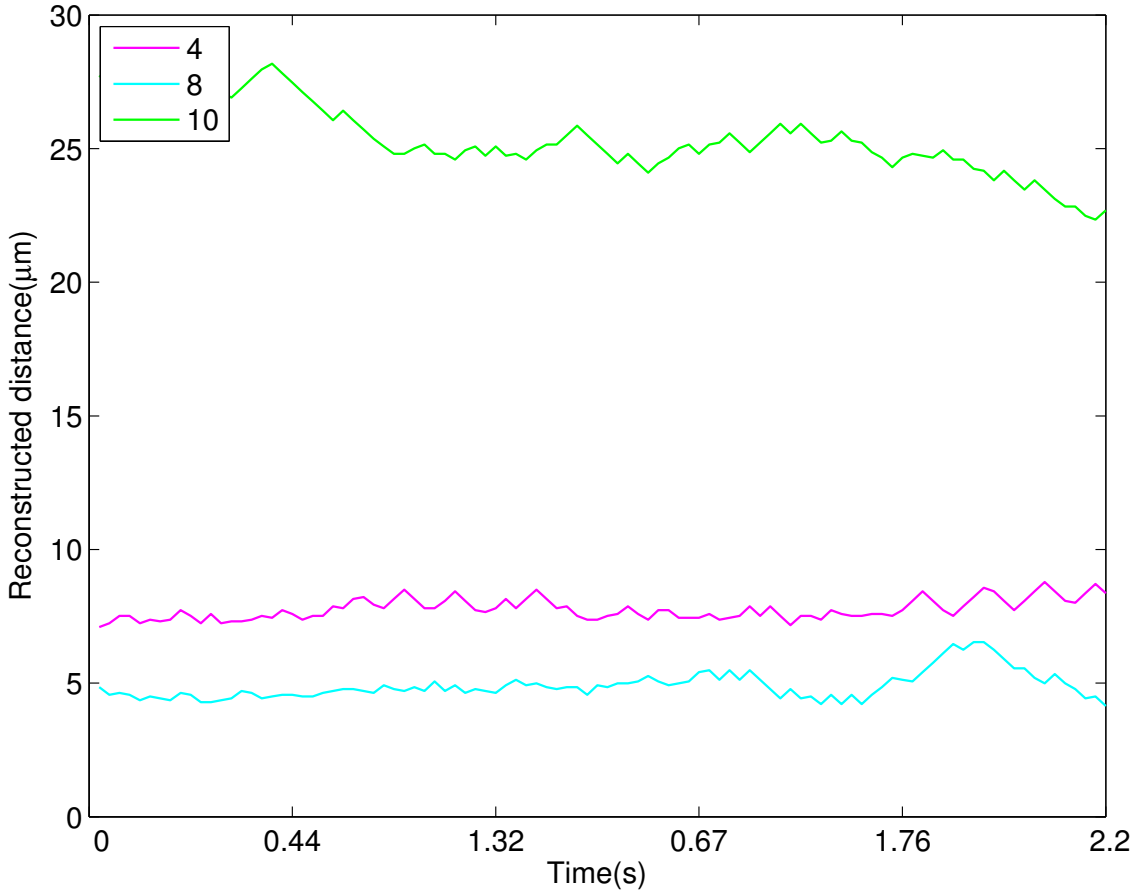

Figure 9: Reconstructed distance for three objects over time.

Fig. 10 shows the reconstructed distance for object 4, 5 and 6. The average reconstructed positions are: for object 4: 7.76 ± 0.08 μm; for object 5: 5.62 ± 0.02 μm; and for object 6; 6.24 ± 0.03 μm.

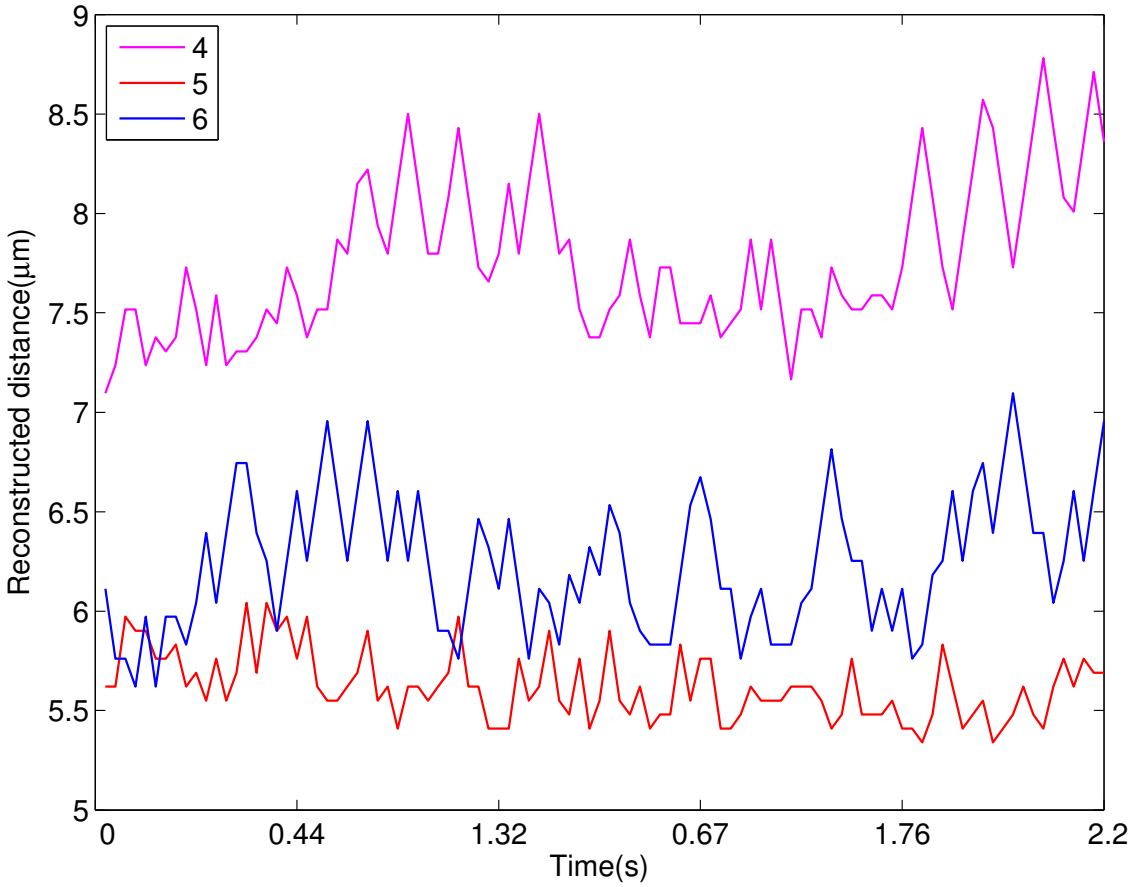

Figure 10: Reconstructed distance for the three objects that were undisturbed.

The reconstruction algorithm was run on a Intel core i7-3770 at 3.4 GHz, and the time to track the objects was 3.3 seconds per object and frame with the z position on the previous frame known, and 12.7 seconds per object and frame when the z position of the previous frame was unknown. In comparison to the original code, this new algorithm was 96% faster.

6.1 Tracking flowing object

To further test the tracking, moving micro-spheres were analyzed. The pump was set to syringe 100 μl, as fast as it could do, 10 times, to get as little motion blur as possible in the images, the images were taken after the last syringe. The micro-fluidic chamber was placed so that the camera could record the edge of the channel in order to quantify edge effects.

Due to readout noise in the high speed camera, the algorithm had to be changed so that the image were subtracted from the background image, instead of the other way around. The frame rate of the camera was set to 200 frames per second and the conversion factor was found to be 0.131 ± 0.008 μm.

Fig. 11 shows the first frame in the image sequence, with its background subtracted, where the detected centers were marked, one can see that the high speed camera had more readout noise. The edge of the channel can be seen as a bright line, in the bottom of the image. As shown in the figure the tracking algorithm generated more than one detections for a single object for some of diffraction patterns and there were also diffraction patterns that were not detected.

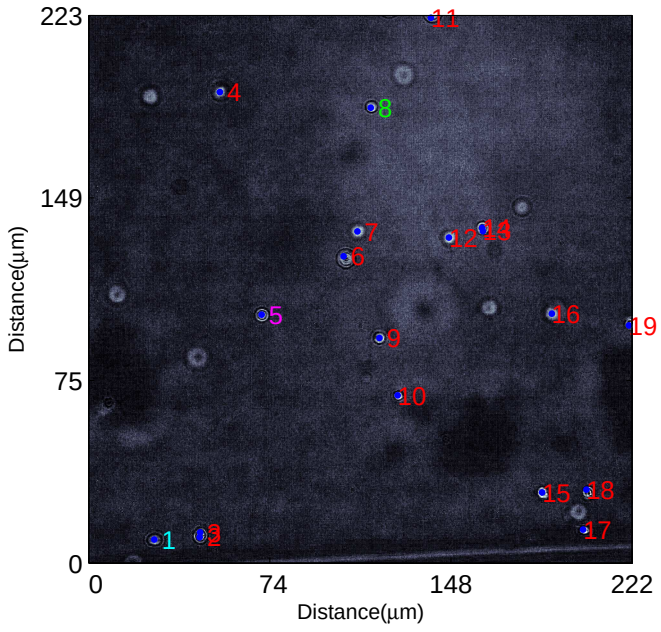

Figure 11: The first frame in the image sequence with flowing objects. The detected centers are marked with a blue dot.

Fig. 12 shows the trajectory of object 1, 5 and 8 in the x, y plane. The flow direction is shown by the blue arrows and as one can see the trajectory of the microspheres do not follow the flow direction since the camera was not perfectly aligned with the flow chamber.

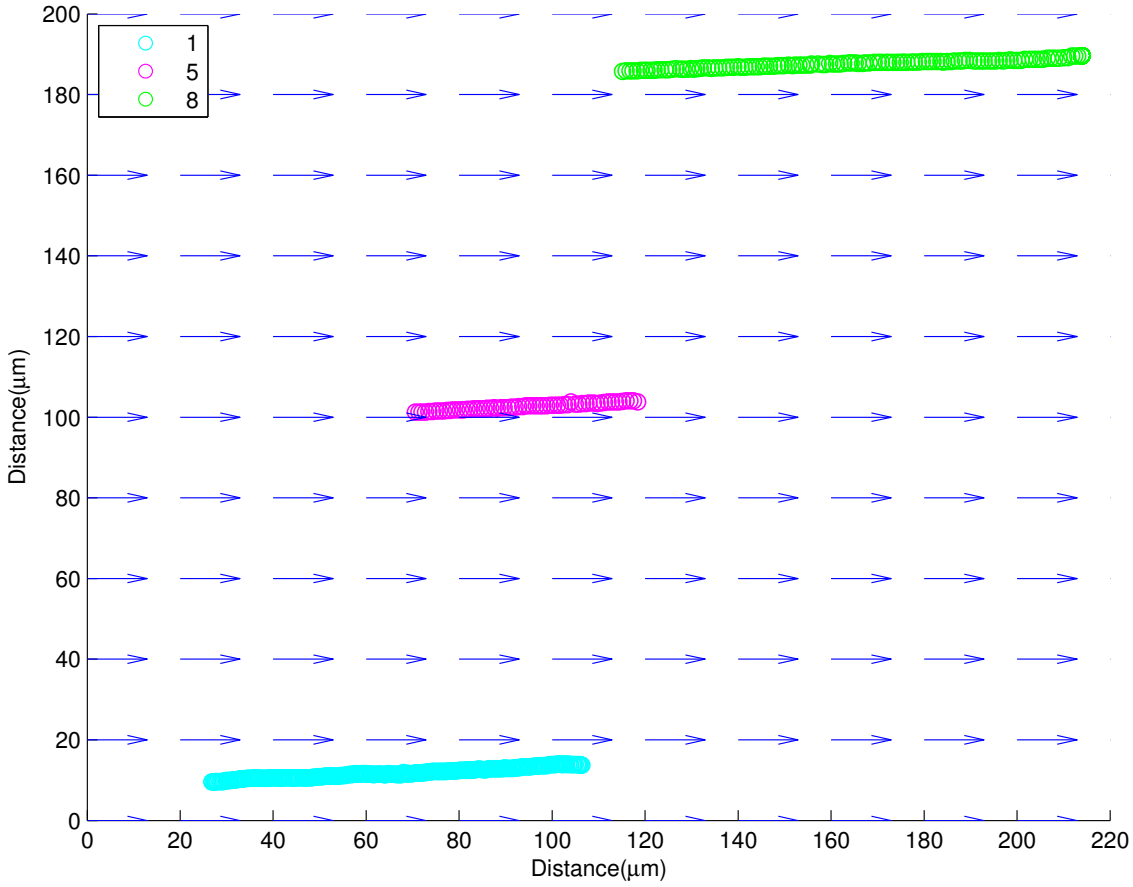

Figure 12: The two dimensional trajectory of three of the objects.

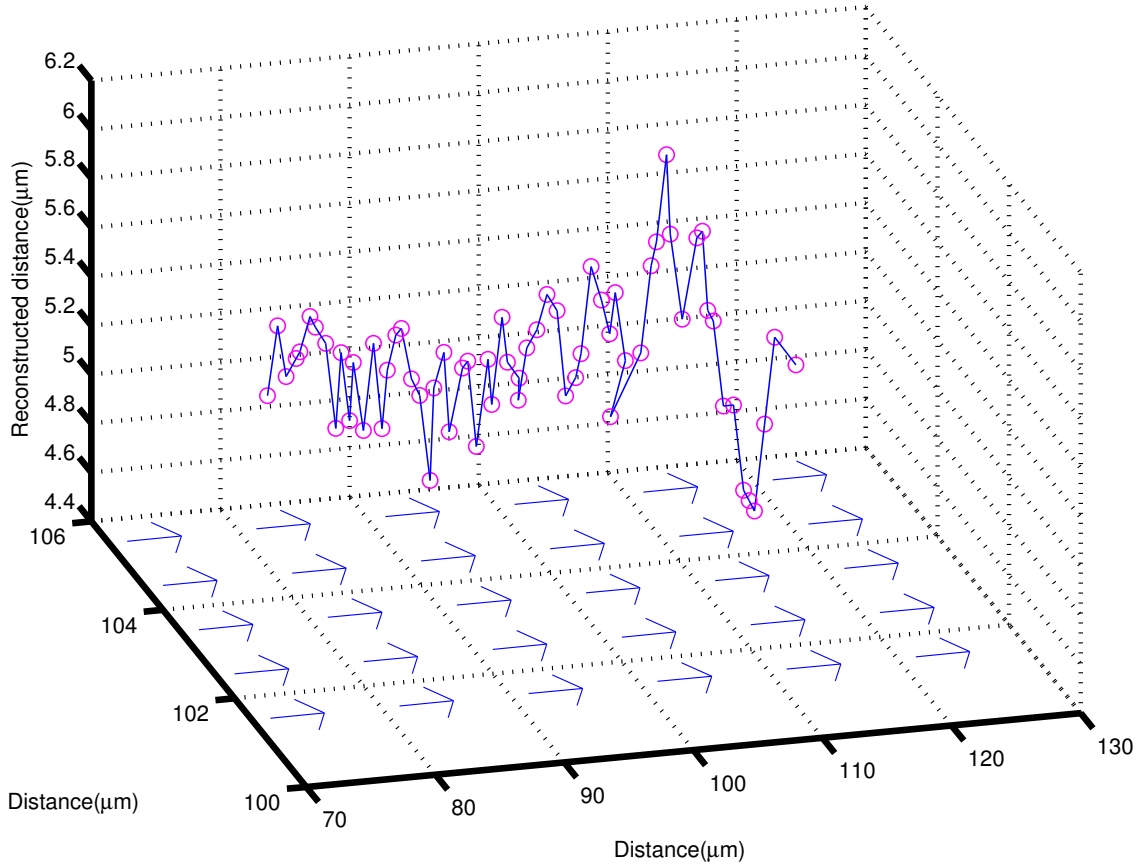

Figure 13: The three dimensional trajectory of object 5.

Fig. 13 shows the three dimensional trajectory for object 5 with a blue line that connects the detected positions from frame to frame. The blue arrows shows the flow direction.

Fig. 14 shows the speed over time for object 1, 5 and 8. A 10 point moving average filter was applied to smooth the data (solid line) and the dotted lines shows the raw data. One can see that object 1 has a lower average speed, 60 ± 2 μm/s, than object 5, 153 ± 4 μm/s and 8, 159 ± 5 μm/s.

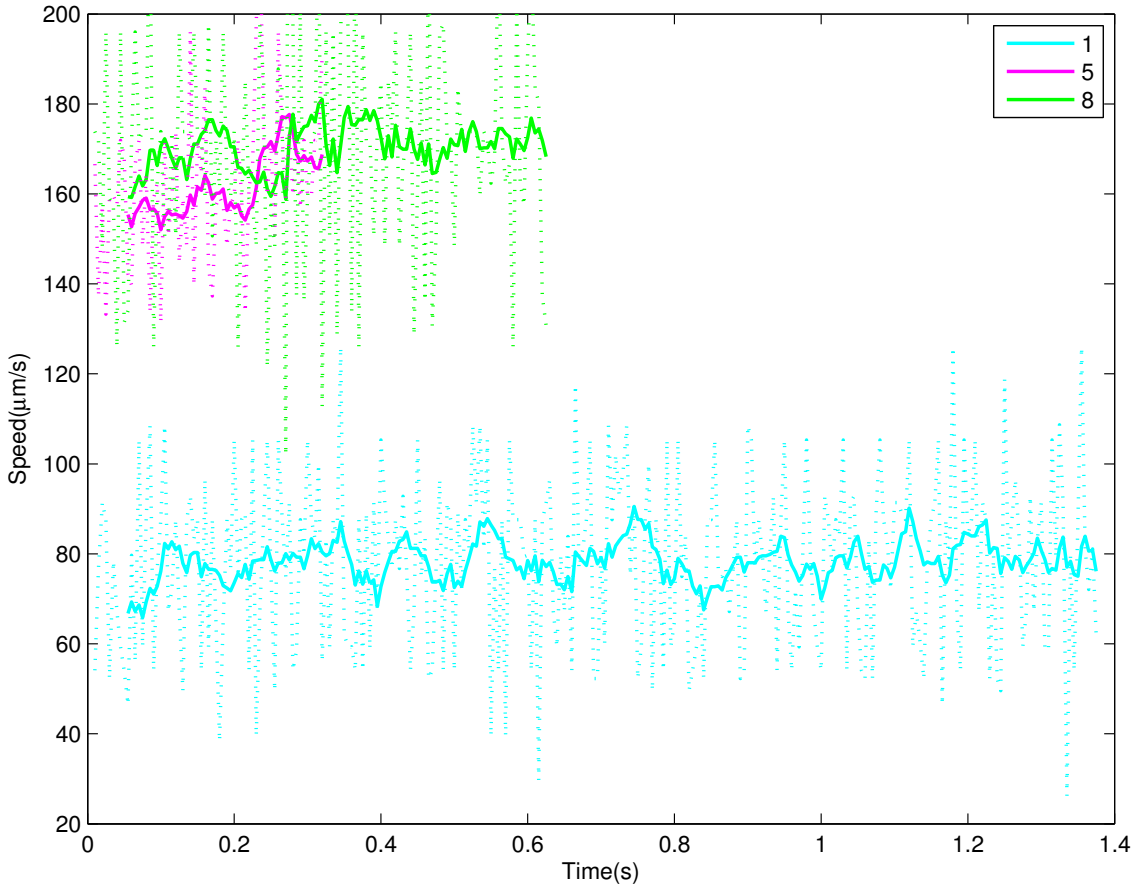

Figure 14: The speed and moving average speed over time.

Fig. 15 shows the reconstructed distances over time, for object 1, 5 and 8. One can see that object 8 has a large motion in the z direction. The average reconstructed distance were 2.19 ± 0.06 μm for object 1, 5.55 ± 0.08 μm for object 5 and 8.4 ± 0.2 μm for object 8.

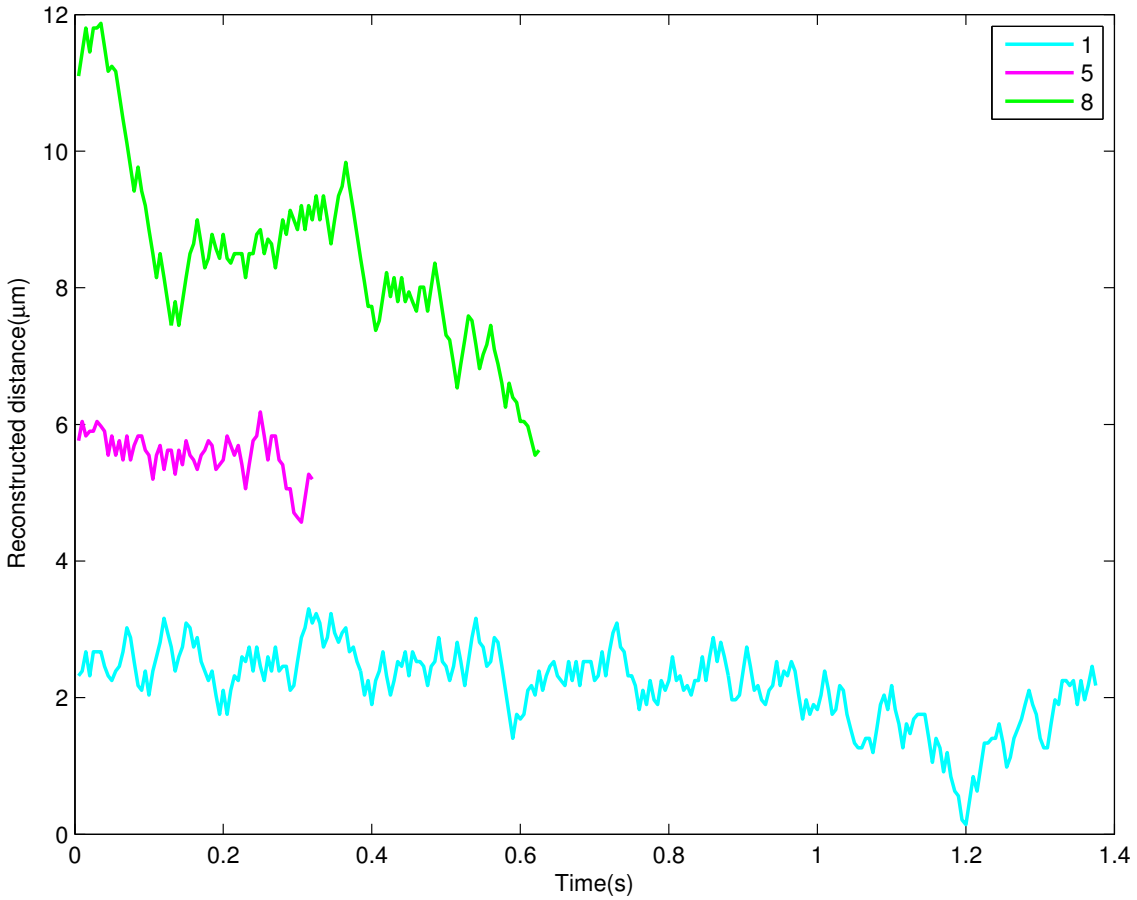

Figure 15: The reconstructed distance over time for three objects.

The tracking algorithm could not track object 5 and 8 for the whole interval since object 5 was not detected in each frame and since object 8 left the field of view.

By tracking objects in the flow, it is possible to estimate the flow profile of the flow. In our setup we could see approximately 220 μm across the channel, which is a bit over half of the width of the channel. Fig. 16 shows a quadratic fit between distance to the edge of the chamber, reconstructed distance and flow speed. The maximum flow speed is found at 170 μm from the edge and at low reconstructed distance, the effect from the reconstructed distance is not statistically significant.

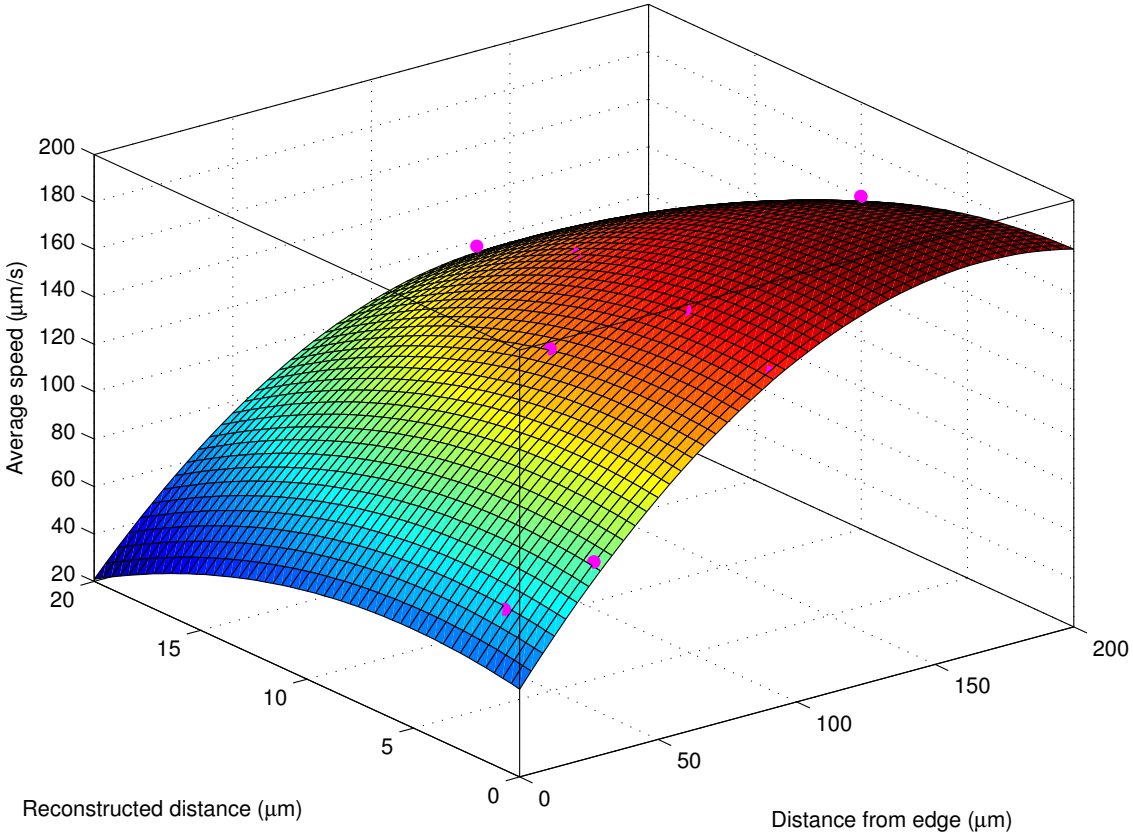

Figure 16: A quadratic fit between the distance from the edge of the channel and the speed of the flow.

6.2 Performance of the algorithm

Fig. 6 show the linear fit of the synthetic hologram, by adding random Gaussian noise, with a standard deviation that is half of the difference between the maximum and minimum intensity of the hologram, the sensitive to noise of the algorithm can be quantified. A fit using a linear model gave a R^2 of 0.9996, meaning as long as the center is accurately found noise is not significantly affecting the reconstruction. The hologram with added Gaussian noise with a standard deviation of 200 can be seen in Fig. 17. Noise in the image may also result that the center of the diffraction pattern is not detected exactly. To test how this affect the reconstruction a synthetic hologram without noise was reconstructed where the detected centers had been randomly moved a few pixels. This resulted in that the linear fit only gave a R^2 of 0.9595,this correspondes to a noticeable deviation of a few μm.

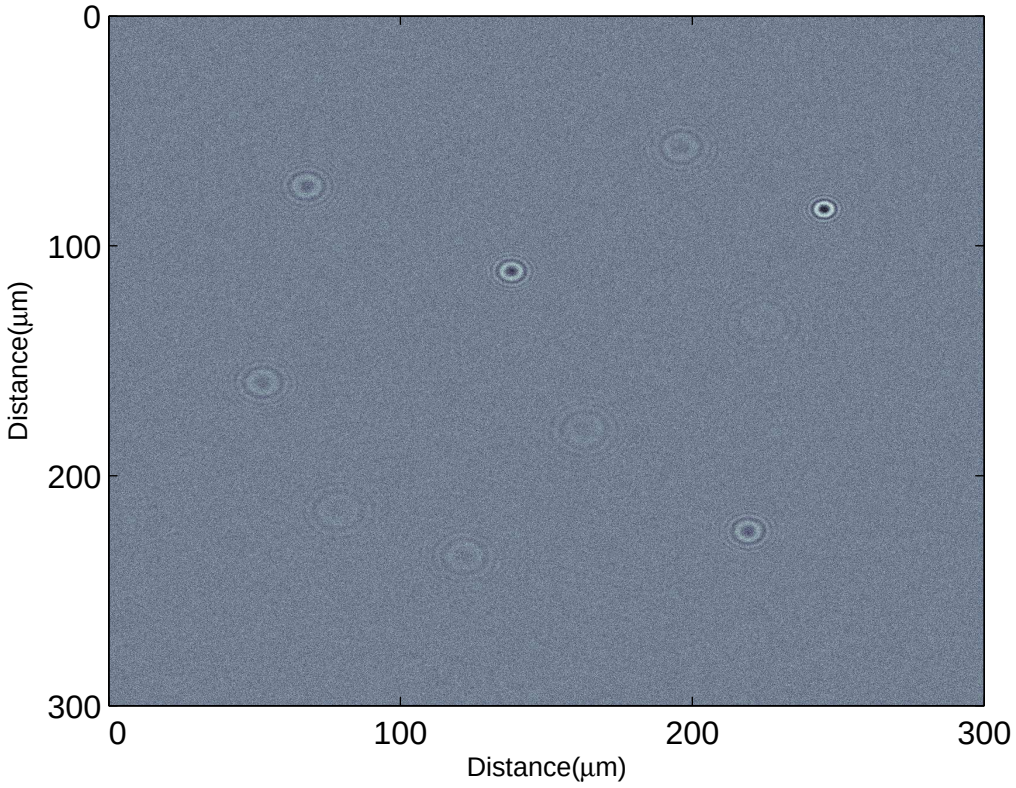

Figure 17: The synthetic hologram with added noise.

In both Fig. 9, 10 and 15 one can see variation in the reconstructed distance, there is a discretization error in the reconstruction algorithm of 70 nm. To analyze how this discretization effects the reconstruction, object 5 in Fig. 11 was tracked using different resolution in the reconstruction. It was found that the resolution used in the reconstruction had little influence on the reconstructed distance, that was 5.54 ± 0.08 μm for both a resolution of 100 nm and 1 nm.

7 Discussion and conclusion

The aim of this work was to develop a three dimensional tracking algorithm based on DHM and to develop an experimental setup able to measure holograms from a micro-fluidic chamber. Holograms from both simulated and experimental data were analyzed and it was found that the cross correlation algorithm, used to track the two dimensional position works well, but it was not always able to detect all micro-spheres in a flow chamber. The reason for this was the overlapping of multiple diffraction patterns when micro-spheres were close and that some of the diffraction patterns were diffuse. A suggestion to improve this detection is to use a more robust approach to detect circular features, as suggested in [22] or by detecting the position of the particles using a symmetry approach [23].

The reconstruction algorithm could predict the position of the object with high accuracy, as seen in Fig. 6, where the linear fit is almost perfect. However, it is important to enclose an area that is big enough to cover the entire diffraction pattern, otherwise the reconstructed distance might be incorrectly determined.

Large diffraction patterns that could not completely be seen, that is, the circular shape was cut in an image due to the finite field-of-view of the camera was, however, problematic. To prevent such problems diffraction patterns at the edge of the hologram were excluded when the reconstruction were made. Overlapping diffraction patterns were also handled this way. This was a fast and secure way to prevent problems with the reconstruction, but as seen in Fig. 7(a) and Fig. 9 undetected objects can still create problems with the reconstruction, which can be seen in the movements in object 8. Diffusive diffraction patterns like the one for object 10, also give rise to similar problems.

From the results it was found that the tracking algorithm gives a detailed view of a particles position and thereby velocity in three dimensions, see Fig. 13. Due to insufficient alignment between the flow chamber and the camera the trajectory seen in Fig. 12 do not follow the marked flow direction. This is shown in Fig. 14 when analyzing the velocity data. Object 1 that is closer to the edge of the channel is moving at a slower velocity, 60 ± 2 μm/s, than the two objects 5 and 8, which moved at a velocity of 153 ± 4 μm/s and 159 ± 5 μm/s, respectively. This is expected since particles closer to the edge will experience a lower fluid velocity when positioned in a laminar flow.

In general, stationary objects were easy to detect since the camera used had a sensitive detector. When analyzing the flowing objects, some micro-spheres could not be detected in some images due to noise most likely originating from the camera used.

By obtaining spatial information in three dimensions it is possible to analyze the flow profile in the channel by plotting the velocity vectors of the tracked micro-spheres as shown in Fig. 16. The fit do not give the peak speed at the center of the channel, like one would expect from equation (17), but with only having information of half of the channel, one can not expect to get better results in the x, y plane and no reference level were taken for the reconstructed distance, so 0 reconstructed distance is not likely close to the bottom of the flow chamber. The few data points also results in high uncertainty in the fitted polynomial, to get a better fit more data is needed.

There are limitations in the algorithm that is strongly connected to noise in the hologram and the finite resolution used in the reconstruction of the objects. It was found that bad center position determination of the diffraction pattern resulted in a noticeable error, while noise in the image during reconstruction and the resolution in the reconstruction had negligible effect on the accuracy of the algorithm.

From equation (1) a conjugate image will also appear on the hologram that will distort the image. With the sample used in this work, the conjugate image will be completely out of focus, therefore we did not need to consider this effect. However, this will not be true for very weakly diffractive objects.

To remove the conjugate image, one must use an off-axis configuration[1][24][25][26]. One should also note that the reconstructed distance will not only depend on the distance, because the shape and refractive index of the object will affect where the focus will be located. The optical path length can be calculated using the phase, making it possible to get the refractive index and thickness of the object, but coupled together[9]. In addtion, by using the real part of the amplitude at the center of the object, one can get the shape of the object[8]. One must also remember to place the object at a proper position so that the focus is between the object and the imaging plane, otherwise the reconstruction will not provide the same result.

In conclusion, this work investigated using DHM and cross correlation to track the three dimensional position of objects, using a simple setup. It was found that it was possible to track the position with high accuracy, as long as the diffraction pattern was clear and there were no other diffraction pattern close to it. This was verified using micro-spheres in both stationary and flowing fluid. The approach presented can thus be used to track individual objects or study the profile of a flow and a future application is to track cells or bacteria using this algorithm. A future development of this technique is to refine the algorithm to handle *E. coli* cells to allow for studies of bacterial adhesion under fluid flow[27].

A Saved data

The tracks will be saved as .txt files in a folder called `.\Output\Tracks` and will have layout according to Table 1, the velocity take three rows, one for each component in spherical coordinates, any value that was not calculated is given a value of NaN.

Table 1: Layout of the output file, with example data

Frame number	y position	x position	Velocity of the object			Reconstructed distance
1	31.368	53.587	NaN	NaN	NaN	11.1
2	31.368	54.24	148.38	1.5708	1.0776	11.451
3	31.107	54.894	157.33	-1.903	1.10079	11.803
4	31.237	55.417	108.69	1.3258	1.4412	11.873
5	31.237	56.07	142.27	1.5708	1.9769	11.592
6	NaN	NaN	NaN	NaN	NaN	NaN
7	NaN	NaN	NaN	NaN	NaN	NaN
8	NaN	NaN	NaN	NaN	NaN	NaN

B Functions used

Function name	Use
test_track	Base function for tracking
Object_detection	Algorithm to detection diffraction pattern
show_image	Show the hologram and binary mask to the user
Object_tracking	Algorithm to update the x y position
Fre2_kri2_reco_Frame	Algorithm to reconstruct the z position, when the z position is not known in the previous frame
Fre2_kri2_reco_Frame_Tune	Algorithm to reconstruct the z position, when the z position is known in the previous frame
plot_flow	Script to plot reconstructed distance and speed over time and trajectory of the objects
plot_speed	Script to get the flow profile of a flow chamber

The plot scripts and show_image generate figures that may need to be manually changed depending on the data.

References

[1] M. K. Kim, "Principles and techniques of digital holographic microscopy," *SPIE Reviews*, vol. 1, no. 1, p. 018005, 2010.

[2] F. Shen and A. Wang, "Fast-Fourier-transform based numerical integration method for the Rayleigh-Sommerfeld diffraction formula.," *Applied optics*, vol. 45, no. 6, pp. 1102–1110, 2006.

[3] G. D. Gillen and S. Guha, "Modeling and propagation of near-field diffraction patterns: A more complete approach," *American Journal of Physics*, vol. 72, no. 9, p. 1195, 2004.

[4] F. Dubois, C. Schockaert, N. Callens, and C. Yourassowsky, "Focus plane detection criteria in digital holography microscopy by amplitude analysis.," *Optics express*, vol. 14, no. 13, pp. 5895–5908, 2006.

[5] L. Ma, H. Wang, Y. Li, and H. Jin, "Numerical reconstruction of digital holograms for three-dimensional shape measurement," *Journal of Optics A: Pure and Applied Optics*, vol. 6, no. 4, pp. 396–400, 2004.

[6] J. T. Cheng, A. a. Aarnisalo, E. Harrington, M. D. S. Hernandez-Montes, C. Furlong, S. N. Merchant, and J. J. Rosowski, "Motion of the surface of the human tympanic membrane measured with stroboscopic holography," *Hearing Research*, vol. 263, no. 1-2, pp. 66–77, 2010.

[7] G. Popescu, "Spatial light interference microscopy (SLIM)," *IEEE Photonic Society 24th Annual Meeting, PHO 2011*, vol. 19, no. 2, p. 797, 2011.

[8] J. Zakrisson, S. Schedin, and M. Andersson, "Cell shape identification using digital holographic microscopy," *Applied Optics*, vol. 54, no. 24, p. 7442, 2015.

[9] B. Rappaz, P. Marquet, E. Cuche, Y. Emery, C. Depeursinge, and P. Magistretti, "Measurement of the integral refractive index and dynamic cell morphometry of living cells with digital holographic microscopy.," *Optics express*, vol. 13, no. 23, pp. 9361–9373, 2005.

[10] F. Dubois, C. Yourassowsky, O. Monnom, J.-C. Legros, O. Debeir, P. Van Ham, R. Kiss, and C. Decaestecker, "Digital holographic microscopy for the three-dimensional dynamic analysis of in vitro cancer cell migration.," *Journal of biomedical optics*, vol. 11, no. 5, p. 054032, 2006.

[11] D. Merrill, R. An, H. Sun, B. Yakubov, D. Matei, J. Turek, and D. Nolte, "Intracellular Doppler Signatures of Platinum Sensitivity Captured by Biodynamic Profiling in Ovarian Xenografts," *Nature Publishing Group*, no. August 2015, pp. 1–7, 2016.

[12] K. Alm, H. Cirenajwis, L. Gisselsson, A. G. Wingren, B. Janicke, A. Mölder, S. Oredsson, and J. Persson, "Digital Holography and Cell Studies," *Holography, Research and Technology*, pp. 237–252, 2011.

[13] V. Micó, J. García, Z. Zalevsky, and B. Javidi, "Phase-shifting gabor holographic microscopy," *IEEE/OSA Journal of Display Technology*, vol. 6, no. 10, pp. 484–489, 2010.

[14] M. K. Cheezum, W. F. Walker, and W. H. Guilford, "Quantitative comparison of algorithms for tracking single fluorescent particles.," *Biophysical journal*, vol. 81, no. 4, pp. 2378–2388, 2001.

[15] E. Fallman, S. Schedin, J. Jass, M. Andersson, B. E. Uhlin, and O. Axner, "Optical tweezers based force measurement system for quantitating binding interactions: system design and application for the study of bacterial adhesion," *Biosens Bioelectron*, vol. 19, no. 11, pp. 1429–1437, 2004.

[16] O. Axner, O. Björnham, M. Castelain, E. Koutris, S. Schedin, E. Fällman, and M. Andersson, "Unraveling the Secrets of Bacterial Adhesion Organelles using Single Molecule Force Spectroscopy," *Springer series in chemical physics: single molecule spectroscopy in chemistry, physics and biology*, vol. 96, pp. 337–362, 2010.

[17] O. Axner, M. Andersson, O. Björnham, M. Castelain, J. Klinth, E. Koutris, and S. Schedin, "Assessing bacterial adhesion on an individual adhesin and single pili level using optical tweezers," *Advances in Experimental Medicine and Biology*, vol. 715, pp. 301–313, 2011.

[18] K. Norregaard, M. Andersson, P. E. Nielsen, S. Brown, and L. B. Oddershede, "Tethered particle analysis of supercoiled circular DNA using peptide nucleic acid handles," *Nat. Protocols*, vol. 9, no. 9, pp. 2206–2223, 2014.

[19] K. Norregaard, M. Andersson, K. Sneppen, P. E. Nielsen, S. Brown, and L. B. Oddershede, "DNA supercoiling enhances cooperativity and efficiency of an epigenetic switch," *Proceedings of the National Academy of Sciences*, vol. 110, no. 43, pp. 17386–17391, 2013.

[20] N. Mortezaei, B. Singh, E. Bullitt, B. E. Uhlin, and M. Andersson, "P-fimbriae in the presence of anti-PapA antibodies: new insight of antibodies action against pathogens.," *Scientific reports*, vol. 3, p. 3393, 2013.

[21] M. Andersson, F. Czerwinski, and L. B. Oddershede, "Optimizing active and passive calibration of optical tweezers," *Journal of Optics*, vol. 13, no. 4, p. 044020, 2011.

[22] H. Zhang, K. Wiklund, and M. Andersson, "A fast and robust circle detection method using isosceles triangles sampling," *Pattern Recognition*, vol. 54, pp. 218–228, 2015.

[23] A. Rodriguez, H. Zhang, K. Wiklund, T. Brodin, J. Klaminder, P. Andersson, and M. Andersson, "A robust particle detection algorithm based on symmetry," *arXiv:1605.03328*, 2016.

[24] U. Schnars and W. Juptner, "Digital recording and numerical reconstruction of holograms," *Institute of Physics Publishing*, vol. 13, p. 17, 2002.

[25] J. Weng, J. Zhong, and C. Hu, "Digital reconstruction based on angular spectrum diffraction with the ridge of wavelet transform in holographic phase-contrast microscopy.," *Optics express*, vol. 16, no. 26, pp. 21971–21981, 2008.

[26] W. Zhang, M. Wang, M. Zheng, and J. Wu, "An effective approach to removing zero-order term overlap and controlling image distortion in digital off-axis holography," *Optics Communications*, vol. 356, pp. 589–594, 2015.

[27] J. Zakrisson, K. Wiklund, O. Axner, and M. Andersson, "Helix-like biopolymers can act as dampers of force for bacteria in flows," *European Biophysics Journal*, vol. 41, no. 6, pp. 551–560, 2012.